

## Elastic FWI of multi-component ocean-bottom seismic to update shear-wave velocity models

N. Masmoudi<sup>1</sup>, A. Ratcliffe<sup>1</sup>, O. Bukola<sup>1</sup>, J. Tickle<sup>1</sup>, X. Chen<sup>1</sup>

<sup>1</sup> CGG

### Summary

---

Elastic full-waveform inversion (FWI) is now emerging as an industrial tool for the compressional velocity ( $V_p$ ) model build, driven mainly by diving and reflected P waves. On the other hand, the inversion of S waves in elastic FWI to update shear velocity ( $V_s$ ) models is more challenging due to the limitations of data acquisition and reduced sensitivity of surface seismic to  $V_s$ . In this paper, we propose a practical methodology for low-wavenumber  $V_s$  updates by elastic FWI, driven mainly by converted waves in multi-component ocean-bottom seismic data. The first key step of our methodology builds a high-quality  $V_p$  model from elastic  $V_p$  FWI using the hydrophone and vertical geophone data. The second key step is the use of horizontal geophones to reconstruct the low wavenumbers of the  $V_s$  model from the kinematics of the converted waves. We show a field application of our approach highlighting improved PS reverse time migration (RTM) imaging, and better consistency with the PP RTM, coming from the elastic  $V_s$  FWI. In addition, a  $V_s$  update from a Born-based PS-reflection FWI method also shows a good PS RTM uplift, although the elastic FWI model generated the better PS RTM image.

## Elastic FWI of multi-component ocean-bottom seismic to update shear-wave velocity models

### Introduction

Recent applications have shown the success of elastic full-waveform inversion (FWI) as a compressional velocity ( $V_p$ ) model building tool in areas with large impedance contrasts (Plessix and Krupovnickas, 2021; Wu et al., 2022; Masmoudi et al., 2023; Richardson et al., 2023) or for directly estimating elastic properties ( $V_p$ , shear velocity ( $V_s$ ) and density) for detailed reservoir characterization (Wang et al., 2021). Both applications, so far, are mainly driven by diving and reflected P waves. Indeed, in marine applications the predominant elastic approach inverts  $V_p$  using hydrophone data, hence with minimal contamination from converted waves, assuming a fixed  $V_s/V_p$  derived from petrophysics relations and geological/well information. Despite the inherent uncertainty in  $V_s/V_p$ , the success of these applications indicates the robustness of  $V_p$  inversions to errors in the background  $V_s$  models (Cho et al., 2022; Masmoudi et al., 2022).

Ocean-bottom seismic (OBS) surveys with hydrophone and three component geophones record both P- and S-waves. Deriving accurate  $V_s$  background models is particularly pertinent when migrating PS converted-wave data, where these PS images can help characterize the elastic properties of reservoirs, identify fluid contacts, and illuminate targets beneath gas zones. Traditional approaches to  $V_s$  model building include PP-PS event registration and joint tomography. However, these techniques are often impeded by the lack of a reliable PS image in the shallow part of the model due to the sparse-receiver acquisition of typical OBS surveys and face the traditional limitations of ray-based tomography. The prospect of using elastic FWI to update  $V_s$  is highly attractive (Sears et al., 2008; Vigh et al., 2014), but comes with its own challenges: 1) the computational cost of shear-wave simulation, 2) the lack of sensitivity of surface seismic to long  $V_s$  wavelengths, and 3) multi-parameter crosstalk (Cao et al., 2022). To mitigate some of these challenges, Masmoudi et al. (2021) proposed a PS-reflection FWI (PS-RFWI) method for updating the background  $V_s$  using processed PS data and acoustic Born modelling. More recently, Cho et al. (2022) proposed an elastic  $V_s$  FWI strategy driven by the reflected converted-waves from the top salt interface recorded in horizontal OBS components.

In this abstract, we extend the elastic FWI of Masmoudi et al. (2023) to multi-component geophone data, with an emphasis on the horizontal components for  $V_s$  updates. Our method assumes good  $V_p$  reconstruction from FWI of hydrophone and, optionally, vertical geophone data. Similar to Cho et al. (2022), our method uses converted waves generated from a strong and fixed elastic boundary, a chalk package in our field data example, to drive the  $V_s$  update. Our application on a North Sea OBS data set shows improvement in the PS reverse-time migration (RTM) image in terms of event continuity and alignment with the PP RTM. Further, a comparison of our elastic  $V_s$  FWI against the acoustic-based PS-RFWI shows that elastic FWI consistently gives a better result.

### Elastic $V_s$ FWI methodology using multi-component OBS data

Carefully designed synthetic experiments allow  $V_p$  and  $V_s$  reconstruction from FWI using geophone, or even hydrophone, data alone (Sears et al., 2008). For field data applications, many challenges arise due to acquisition and data limitations, making workflows essential for successful inversions of both parameters. Robust  $V_p$  FWI reconstruction can be obtained from marine seismic surveys (including OBS) due to long offsets, low frequencies, and the strong data sensitivity to  $V_p$ . Obtaining an equivalent  $V_s$  model from FWI requires much longer offsets and recording times to capture the S-diving waves essential for background reconstruction, and even lower frequencies to accommodate the shorter spatial wavelength due to the slower  $V_s$ . Hence, the long-wavelength model is a key challenge of  $V_s$  inversions.

Given these issues, the first step in our  $V_s$  inversion workflow is to obtain an accurate  $V_p$  model, for both low- and high-wavenumber components, through an elastic FWI of hydrophone and vertical geophone recordings. The starting  $V_s/V_p$  for this inversion is built from petrophysics relations and adjusted according to geological knowledge and any available well information. This  $V_p$  inversion is generally robust to  $V_s/V_p$  inaccuracies. However, when excessive  $V_s$  errors exist around large velocity contrasts, this can damage the elastic  $V_p$  inversion (Masmoudi et al., 2022). Throughout this first inversion,  $V_s$  is updated passively via the velocity ratio, allowing the reconstruction of an initial  $V_s$

model that is appropriate for the second step of the workflow. Additionally, the velocity ratio can be improved in this first step, especially when converted waves are generated by strong model contrasts.

The second step in our workflow is a  $V_s$  reconstruction using elastic FWI of horizontal geophone data. The observed geophone data has minimal processing and contains converted waves and multiples. Similar events generated in the modelled data can help stabilize the  $V_s$  inversion. Hence, deriving an initial  $V_s$  model with sufficiently high-wavenumber components from the first step is a central point in our proposed workflow. Since the  $V_s$  inversion is mainly driven by the PS reflection data, a scattering angle filter approach (Alkhalifah, 2015) is used to enhance the tomographic components in the  $V_s$  gradient. Finally, a time-lag cost function is adopted as it can provide a more robust inversion of the kinematics of PS reflections compared to the classical least-squares cost function (Zhang et al., 2018).

### North Sea field data example

We applied our elastic  $V_s$  FWI methodology on a multi-component ocean-bottom-node (OBN) survey from the North Sea, with node spacing of 50 m by 300 m in x and y, respectively. The source is located at 7 m depth with a spacing of 25 m by 50 m in x and y, respectively. This area is characterized by a shallow water environment with a water depth of approximately 100 m, and a hard water bottom contrast creating favourable conditions for a strong P-to-S conversion. Additionally, the model included shallow complexities typical of this region: layers with gas charged accumulations, injectites, and cemented pipes. Finally, the presence of a highly reflective, strong contrast, chalk package at approximately 2800 m depth limited the P-diving wave penetration depth but presented an opportunity as a potent source for generating converted waves.

As a first step, a 25 Hz  $V_p$  FWI model was derived from both hydrophone and geophone data (see Figure 1a), where the  $V_s/V_p$  ratio was obtained from geological and well information. Figures 1b-1e show examples of x and y particle velocity data ( $V_x$  and  $V_y$ ) at 4 Hz, illustrating observed and modelled data from the starting model. Converted waves from the shallow overburden and the deeper chalk layer are indicated by green arrows. These events, in addition to surface waves (blue arrows), are present in the modelled and observed data. Following the  $V_p$  model reconstruction, elastic  $V_s$  FWI was run in a test area up to 10 Hz, utilizing both horizontal geophone components. We initially ran separate  $V_x$  and  $V_y$  updates but achieved better results by simultaneously using both components, hence justifying the extra computational cost needed for the reciprocity scenario that is typically used in OBS acquisitions.

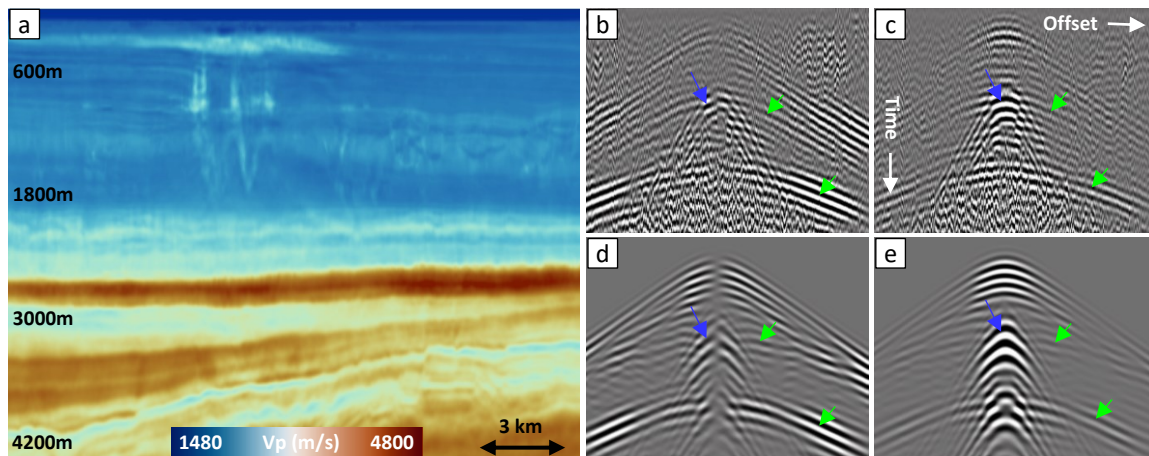


**Figure 1** (a) The 25 Hz  $V_p$  FWI model derived from step 1 of the workflow. Observed and modelled receiver gathers comparison at 4 Hz corresponding to: (b,d)  $V_x$ , and (c,e)  $V_y$  components, respectively.

The 10 Hz elastic  $V_s$  FWI velocity perturbation in Figure 2a shows mainly “rabbit-ear” like low-wavenumber updates driven by the kinematics of the converted waves, with the perturbation also picking some of the shallow anomalies (indicated by the yellow arrow) and the deeper chalk heterogeneities between 1800 m and 3000 m depth. The impact of the  $V_s$  update is assessed on the migrated PS image, shown in Figures 2a and 2b, where some PP interpreted horizons have been overlaid to facilitate the results interpretation. These images, along with the PP-PS interleaved displays in Figures 2c and 2d, clearly show an improved PS RTM following the elastic  $V_s$  FWI update revealing

some of the thin reflectors inside the chalk package, improving the event continuity, as well as yielding better alignment with the PP image (red versus green arrows).

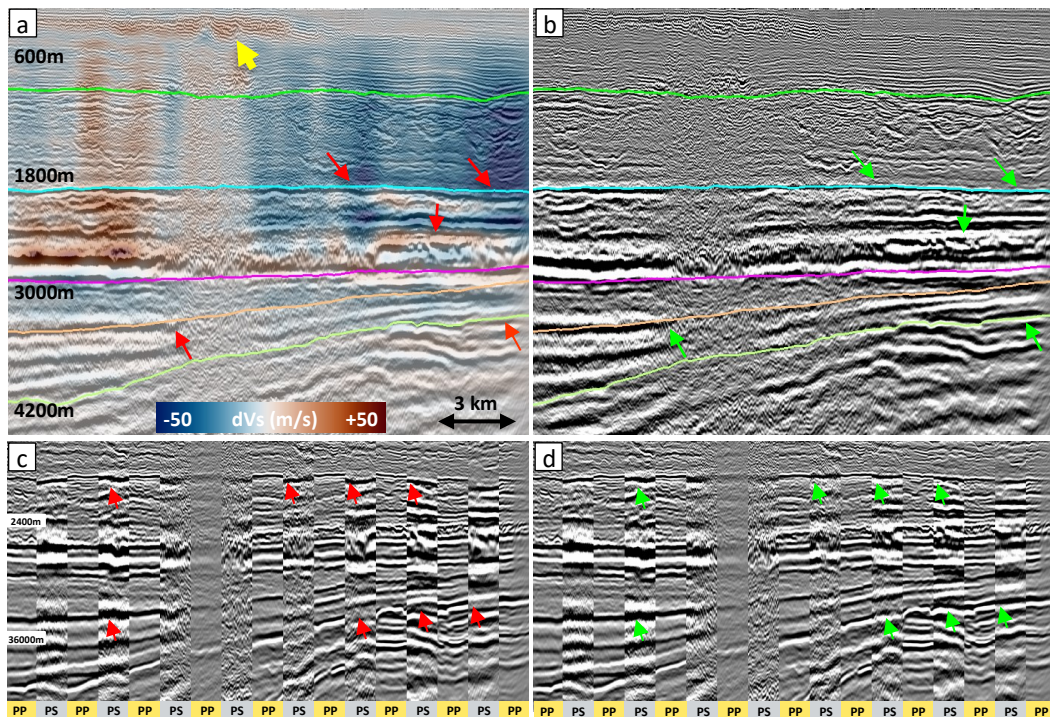


**Figure 2** PS-RTM images using  $V_s$  with key PP horizons overlaid: (a) before, and (b) after elastic FWI. The elastic  $V_s$  FWI perturbation is overlaid on the PS RTM in panel (a). Interleaved display of the PP RTM and PS RTM images where the PS RTM used the  $V_s$  model: (c) before, and (d) after elastic FWI.

### Discussion and comparison with the acoustic-based PS-RFWI

Our proposed elastic  $V_s$  FWI workflow uses some key learnings from PS-RFWI (Masmoudi et al., 2021). In PS-RFWI, the background  $V_s$  is inverted using radially rotated data processed to keep PS-reflections only. Also, PS-RFWI is based on scale separation where a perturbation image and smooth velocity models are provided to an acoustic-based PS Born modelling, allowing explicit computation of the tomographic “rabbit-ear” kernel. To mitigate velocity and reflector depth ambiguity, PS-RFWI assumes accurate (low wavenumber)  $V_p$  models and a migrated PP image for the (high wavenumber) perturbation. Similar to PS-RFWI, our elastic  $V_s$  FWI assumes good reconstruction of  $V_p$ , ideally both low- and high-wavenumbers, such that the high-wavenumbers can play the role of the PS-RFWI reflectivity and generate converted waves via Gardner’s density and velocity ratio relationships. Despite the similarities, there are several benefits of elastic  $V_s$  FWI over PS-RFWI. For one, it is a fully elastic scheme. Also, it uses raw geophone data with minimal processing, hence is not limited by a Born (single-scattering) approach and can use multiples and all converted waves – this can yield improved resolution especially in the shallow. Finally, in theory, there are no wavenumber restrictions with elastic  $V_s$  FWI as it can naturally update both low- and high-wavenumber components, although we note that PS-RFWI was recently extended to generate explicit high-wavenumber updates (Peiro et al., 2022).

We assessed the PS-RFWI update of the  $V_s$  background model on the same field data. When compared with the same interleaved PP-PS RTM display in Figure 2c (using the  $V_s$  starting model), Figure 3a demonstrates an improved PS image following PS-RFWI. The comparison of Figures 3a and 3b shows that both PS-RFWI and elastic FWI technologies, using different data types, achieve similar outcomes. However, the elastic FWI in Figure 3b reveals slightly superior results (green versus orange arrows).

### Conclusions

We proposed a  $V_s$  inversion method based on elastic FWI of multi-component data. Key aspects of the method involve the use of P-waves in hydrophone and vertical geophone recordings for the derivation of a detailed and accurate  $V_p$  model, followed by the use of converted waves in the horizontal components for a  $V_s$  update. The success of the method lies on fixing the PS reflectors depth and

promoting the tomographic components of the  $V_s$  gradient. A North Sea OBN application showed improved PS RTM imaging, and better consistency with the PP RTM. A comparison of elastic  $V_s$  FWI against PS-RFWI reveals a similar PS RTM uplift. This highlights the potential of both technologies to yield reliable  $V_s$  models, although the elastic  $V_s$  FWI model generated the best PS RTM image.

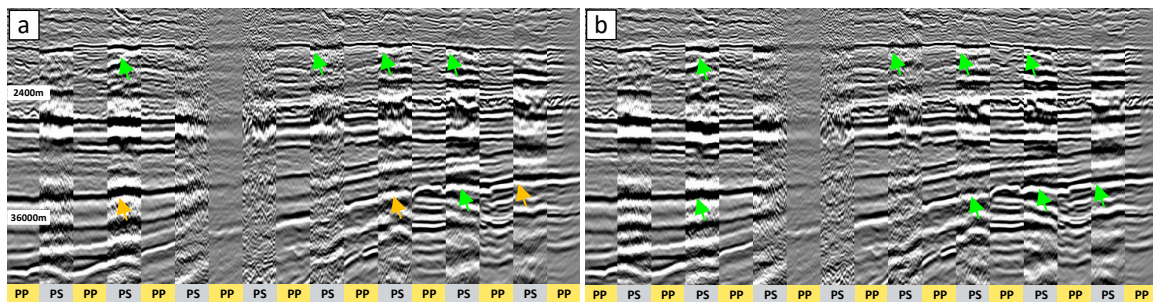


**Figure 3** PP and PS RTM interleaved display where PS RTM used the  $V_s$  model from: (a) PS-RFWI of the processed radial component, and (b) elastic FWI of the raw horizontal components.

### Acknowledgments

We thank Aker BP and their license partners on PL442 (PGNiG) and PL873 (Equinor and PGNiG) for permission to use the data and show the results, and CGG for permission to publish. We also thank Steve Hollingworth for discussion and support.

### References

- Alkhalifah, T. [2015] Scattering-angle based filtering of the waveform inversion gradients. *Geophysics Journal International*, **200**, 363-373.
- Cao, J., Brossier, R. and Metivier, L. [2022] Parameterization analysis in elastic full-waveform inversion of multi-component seismic data. *83<sup>rd</sup> EAGE Conference & Exhibition*, Extended Abstracts.
- Cho, Y., Solano, C.P., Kimbro, J., Yang, Y., Plessix, R-E. and Matson, K. [2022] Influence of shear velocity on elastic full-waveform inversion: Gulf of Mexico case study using multicomponent ocean-bottom node data. *Geophysics*, **87**(5), R391–R400.
- Masmoudi, N., Ratcliffe, A., Wang, M., Xie, Y. and Wang, T. [2021] A practical implementation of converted-wave reflection full-waveform inversion. *82<sup>nd</sup> EAGE Conference & Exhibition*, Extended Abstracts.
- Masmoudi, N., Stone, W., Ratcliffe, A., Refaat, R. and Leblanc, O. [2022] Elastic Full-Waveform Inversion for Improved Salt Model Building in the Central North Sea. *83<sup>rd</sup> EAGE Conference & Exhibition*, Workshop Programme, Extended Abstracts.
- Masmoudi, N., Stone, W. and Ratcliffe, A. [2023] Visco-elastic full-waveform inversion and imaging using ocean-bottom node data. *84<sup>th</sup> EAGE Conference & Exhibition*, Extended Abstracts.
- Peiro, M., Gao, W., Fotsoh, A., Masmoudi, N., Roodaki, A., Ratcliffe, A., Prigent, H., Leblanc, O., Dhelie, P.E., Danielsen, V., Haugen, J.A. and Straith, K.R. [2022] PS Imaging on the Edvard Grieg Field: Application of PS Reflection FWI and FWI Imaging. *83<sup>rd</sup> EAGE Conference & Exhibition*, Extended Abstracts.
- Plessix, R-E. and Krupovnickas, T. [2021] Low-frequency, long-offset elastic waveform inversion in the context of velocity model building. *The Leading Edge*, **40**(5), 342-347.
- Richardson, J., Fu, K., Lu, S., Bai, B., Cheng, X. and Vigh, D. [2023] Elastic full-waveform inversion on Caesar-Tonga – Case study. *The Leading Edge*, **42**(6), 414-420.
- Sears, T.J., Singh, S.C. and Barton, P.J. [2008] Elastic full waveform inversion of multi-component OBC seismic data. *Geophysical prospecting*, 2008, **56**, 843-862.
- Vigh, D., Jiao, K., Watts, D. and Sun, D. [2014] Elastic full-waveform inversion application using multi-component measurements of seismic data collection. *Geophysics*, **79**(2), R63–R77.
- Wang, H., Burtz, O., Routh, P., Wang, D., Violet, J., Lu, R. and Lazaratos, S. [2021] Anisotropic 3D elastic full-wavefield inversion to directly estimate elastic properties and its role in interpretation, *The Leading Edge*, **40**(4), 277-286.
- Wu, Z., Wei, Z., Zhang, Z., Mei, J., Huang, R. and Wang, P. [2022] Elastic FWI for large impedance contrasts, SEG Technical Program Expanded Abstracts: 3686-3690.
- Zhang, Z., Mei, J., Lin, F., Huang, R. and Wang, P. [2018] Correcting for salt misinterpretation with full waveform inversion. *88<sup>th</sup> SEG Annual International Meeting*, Expanded Abstracts, 143-1147.